Robust characterization of fluid flow paths and stress-dependent permeability on field scale modelling of geothermal reservoirs

Pedram Mahzari[1], Ashley Stanton-Yonge Sesnic[1], Catalina Sanchez-Roa[1], Giuseppe Saldi[1], Thomas Mitchell[1], Eric H. Oelkers[1], Vala Hjorleifsdottir[2], Sandra Osk Snaebjornsdottir[3], Thomas Ratouis[2], Alberto Striolo[4], Adrian P. Jones[1]

[1]*Department of Earth Sciences, University College London, UK*
[2]*OR, Reykjavik Energy, Iceland*
[3]*Carbfix, Iceland*
[4]*Chemical Engineering, University College London, UK*

Abstract

The Husmuli zone of SW-Iceland Hellisheidi geothermal field is currently being used for re-injection of geothermal fluids and geothermal CO_2 for permanent storage in the form of carbonate minerals. Fully coupled hydro-thermo-mechanical numerical modelling was employed to investigate the coupled impacts of these complex processes on calibration of the fluid flow paths, which can have significant implications for the long-term performance of this subsurface reservoir.

Employing a combination of high-resolution fault mapping with laboratory measurements of stress dependent permeability coupled into a dual porosity field-scale model, the flow paths were calibrated using results of tracer tests performed at the site using stress-dependent permeability tensors. Although vertically extended faults are the primary fluid flow paths, fractures connecting the faults can play an important role in chemical transport. As the upward flow streamlines manifest, deep geological layers can also deviate the fluid flow towards the shallower layers provoking the vertical flow of geothermal fluids, which highlights the sweet spot for sustainable flow and heat extraction in vicinity of faults intercepting the geological layers at depth of 1100 m.

It was also shown that the inclusion of the geomechanical calculations in history matching of the tracer test can lead to change in arrival time and peak of the tracer profiles. Results of an independent tracer test were used to validate the model and demonstrated a reliable predictive capability for the calibrated model, which verifies the consistency of our methodology to incorporate the stress-dependent permeability. The results of this comprehensive modelling study provide insight into the likely fluid flow paths, which can have profound impact on evaluation of various processes such as CO_2 mineralisation taking place in Hellisheidi geothermal reservoir.

Introduction

Harnessing the geo-energy from geothermal reservoirs can be an attractive alternative for energy transition policies [1]. The long-term performance of geothermal reservoirs depends on

the combined effects of hydrodynamic, thermal, geo-mechanical, and geochemical processes taking place during heat extraction [2]. The role of each process may become more significant at different stages of the geothermal exploitation. Geo-mechanical processes such as stress-dependent fluid flow will influence the system from beginning of production and reinjection, and notably this can provoke induced seismicity, e.g. as reported in Diehl et al. [3].

The fault-fracture network plays an essential role in the long-term performance of geothermal reservoirs in terms of heat extraction and re-injection scenarios. Fracture networks and their connectivity have significant impact on heat extraction efficiency [4], development of the geothermal field [5], long-injectivity [6], geochemical reaction paths [4], and geo-mechanical stress distribution [7]. To identify the major fluid flow paths, a series of tracer tests are usually performed, where a thermally stable tracer is injected into injection wells. The concentration of tracer in the recovered effluent is measured in neighbouring producing wells to generate plots of tracer concentration against time. The tracer arrival time in producing wells and profiles of tracer concentrations can be useful tools to characterise the fluid flow paths. It is a routine practice that, equations governing hydrodynamic flow are only (no geomechanics is involved) used to model tracer test for calibrating fluid flow through fracture networks and matrix/fracture fluid exchange [8]. The usual practice for calibrating the geological model is that the spatial distributions of fracture porosity and permeability are tuned to match the results of tracer tests using hydrodynamic modelling [9]. Having calibrated the fluid flow paths, the geological model can be employed to assess reservoir performance over short and long-time frames.

This study evaluates the performance of the Husmuli re-injection zone and its impact on the Hellisheidi geothermal reservoir in SW Iceland through a coupled hydro-thermo-mechanical model. The geomechanical effects can control the fluid flow and heat extraction from geothermal reservoir from early stages of fluid withdrawal and reinjection [10] [11]. The Hellisheidi geothermal reservoir is utilised for geothermal power production at the Hellisheidi geothermal power plant with capacity of 303 MWe and 200 MWth but the field currently hosts about 60 production and 15 re-injection wells [12]. This geothermal reservoir was selected due to its use in the ongoing CarbFix2 CO_2 storage project, where CO_2-charged water is injected into subsurface basalts to mineralise the injected CO_2 into carbonate minerals [13] [14]. The effectiveness and evaluation of this CO_2 mineralisation method relies on mineral dissolution and precipitation reactions occurring along the fluid flow paths. However, the previous attempts for characterising the fluid paths could not lead to a robust model capable of predicting tracer test field observations [8].

High-resolution fault mapping was combined with laboratory measurements of stress dependent permeability, which then were input into a dual porosity field-scale model. Subsequently, here is this study, the results of a tracer test performed on Hellisheidi reservoir were used to calibrate the model to estimate the fluid flow paths. A new approach is taken in this study combining high-resolution geological modelling with a stress-dependent permeability distribution to match tracer test profiles (as opposed to the conventional methods using only hydrodynamic equations). Including stress-dependent permeability can increase the simulation run time noticeably, it however can lead to a model with high degree of predictive capabilities to capture the fluid paths in a fractured reservoir. After matching the tracer profiles, the calibrated model could be considered for predicting other field observations such as another independent tracer test. The results of this study reveal the importance of geomechanical process-based simulations of tracer tests and the coupled impact of hydro-thermo-mechanical processes on geothermal reservoir development.

Geological description of the subsurface reservoir

The Hellisheidi geothermal reservoir in southwest Iceland (SW Iceland) is located in a divergent plate boundary between the North America and Eurasia plates [15], and in particular, on the triple junction between: the volcanic zones of Reykjanes Peninsula (RP) and Western Volcanic Zone (WVZ); and the transform South Iceland Seismic Zone (SISZ) [16] (as shown in Figure 1). The result is the combination of an extensional tectonic regime dominated by NNE normal faulting coupled with the transform plate boundary and expressed in the form of N-S strike-slip faults.

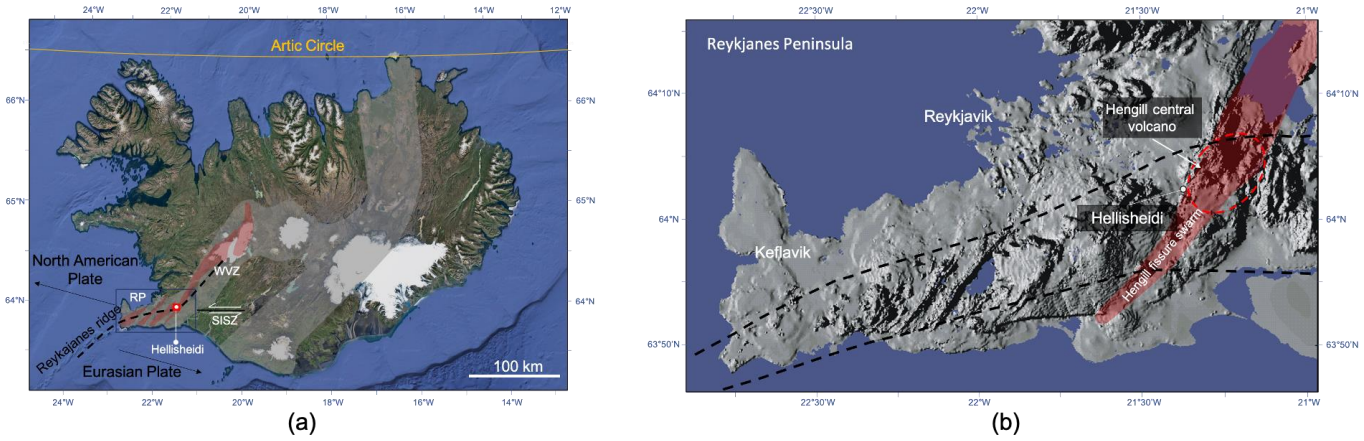

Figure 1: Maps showing location of the study area (a) Active rifting areas in Iceland (light grey) (b) location of the Hengill central volcano (red circle) and associated fissure swarms (red area), modified from Alfresddon et al. [17].

The distribution of wells in the study site are shown in Figure 2 along with geological features of the Husmuli area. A tracer test was performed in June 2013 by injecting 100 kg of tracer

(1,3,6-NTS: naphthalene sulfonates) dissolved in 4 m^3 of water, into the HN17 reinjection well for ~two hours, followed by injection of tracer-free geothermal fluid. The largest quantities of tracer were recovered from the HE31, HE48, and HE44, production wells which serve as monitoring wells and are located northeast of HN17 injection well. The northeast direction of tracer recovery indicates that northeast trending faults are the major contributor to the fluid flow in this system [9]. The concentration of tracer in the collected monitoring wells fluids was measured using high-performance liquid chromatography with a detection limit of 0.2 µG per kg of water [18]. Figure 3a illustrates the temporal variation of tracer concentrations recorded over 200 days. The tracer could be detected at the HE31 well after 14 days of injection [9], and the first appearance of tracer in well HE48 took place after 18 days [9]. Figure 3b illustrates a cross-section of the A-A' plane drawn in Figure 2. As shown, the reservoir consists of several horizontal layers. This is the rationale behind the main gridding scheme for the geological model.

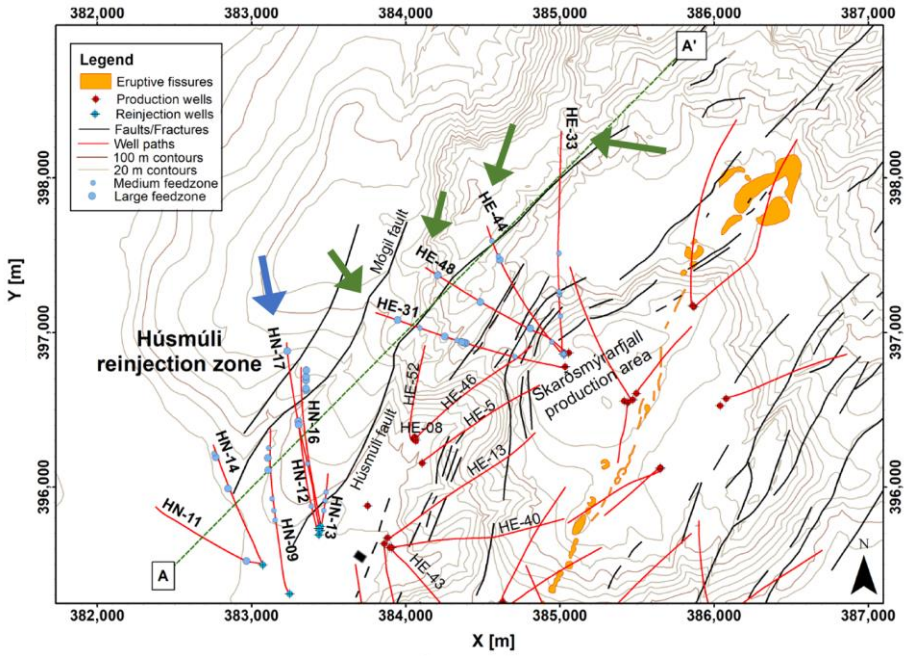

Figure 2: Map of the Husmuli zone of Hellisheidi geothermal reservoir considered in the present study. As highlighted by blue arrows, HN17 well was used for batch tracer injection and producing wells HE31, HE48, HE44, HE33 pointed by green arrows showed the largest tracer recovery, which is modified from the data published in Kristjánsson et al. [18]. The highlighted red dot on Figure 1a points to the location of this map in Iceland.

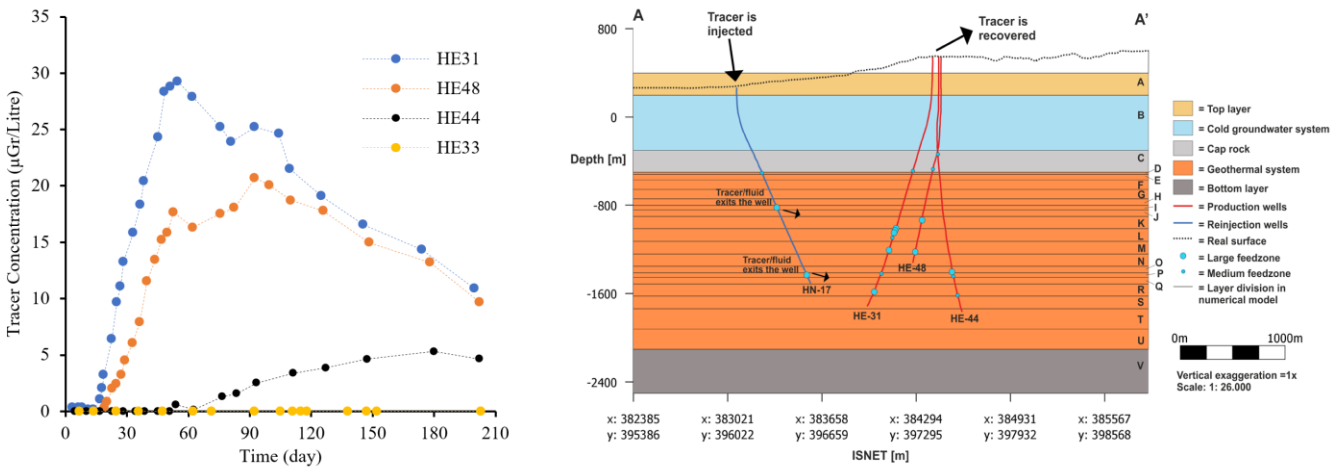

(a) (b)

Figure 3: (a) The temporal evolution of tracer (1,3,6 NTS) concentration recovered in the producing wells indicated in the figure published in Kristjánsson et al [18]. (b) Cross section view of the A-A' plane of the sector (Figure 2) with the feedzones and layers identified, which is modified from Tómasdóttir [19] and Khodayar et al [20]. As the focus of this work is on the tracer test modelling, the relevant wells with significant tracer recoveries are drawn in (b).

Fracture system characterisation

The surface fracture system patterns at the Hellisheidi area were characterised in order to constrain the fluid pathways throughout the reservoir, to be used as input for the numerical simulations. To determine the prevalence of fracture patterns at different scales, fracture mapping and analysis were performed at both the reservoir and outcrop scales. Figure 4 illustrates the Hellisheidi reservoir area with faults and fractures mapped from aerial imagery by Khodayar (2015) [20]. The location of tracer test injection and recovery wells are also indicated in Figure 4a. Fracture pattern quantification toolbox FraqPaQ [21] was used to analyse the fracture system orientation and distribution. Length-weighted fracture strike distribution indicates the predominance of three major fracture systems, oriented NE-ENE, WNW and NS. A fracture density map is shown in Figure 4b, generated by FraQPaQ using the circular scan window method of Mauldon et al. (2001) [22]. Estimated density is shown on a regular grid pattern.

High resolution drone-acquired images of the surface expressions of faults, fractures and dikes were used to construct a photogrammetric model allowing the remote mapping of the governing fracture systems at the outcrop scale. The resulting model with traced fractures is shown in Figure 5a. Traced structures were categorized into 1) Dykes, and 2) Generic fractures. Length-weighted strike orientation indicates a predominance of WNW and NE orientation of generic fractures and ENE orientation for dykes (Figure 5b).

The flow direction indicated by the tracer test suggest that the ENE fracture system, identified both at the reservoir and outcrop scales, imposes a primary control on the fluid transport. Because fluid flow is facilitated where the density and connectivity of fractures are greatest [23], areas of higher surface fracture density might elucidate zones of enhanced fluid flow. A NE-trending, high fracture density zone is identified (Figure 4b), which supports the interpretation of NE direction of fluid pathways. Due to fast breakthrough of tracer in well HE31 (i.e. after 14 days), it is likely that the injected tracer flows directly in a conductive fracture conduit towards HE31 and then the tracer followed a direct path to wells HE48, and HE44. Note that the wells may have feedzones at different depths and in different geological formations, which would affect the tracer flow recovery times.

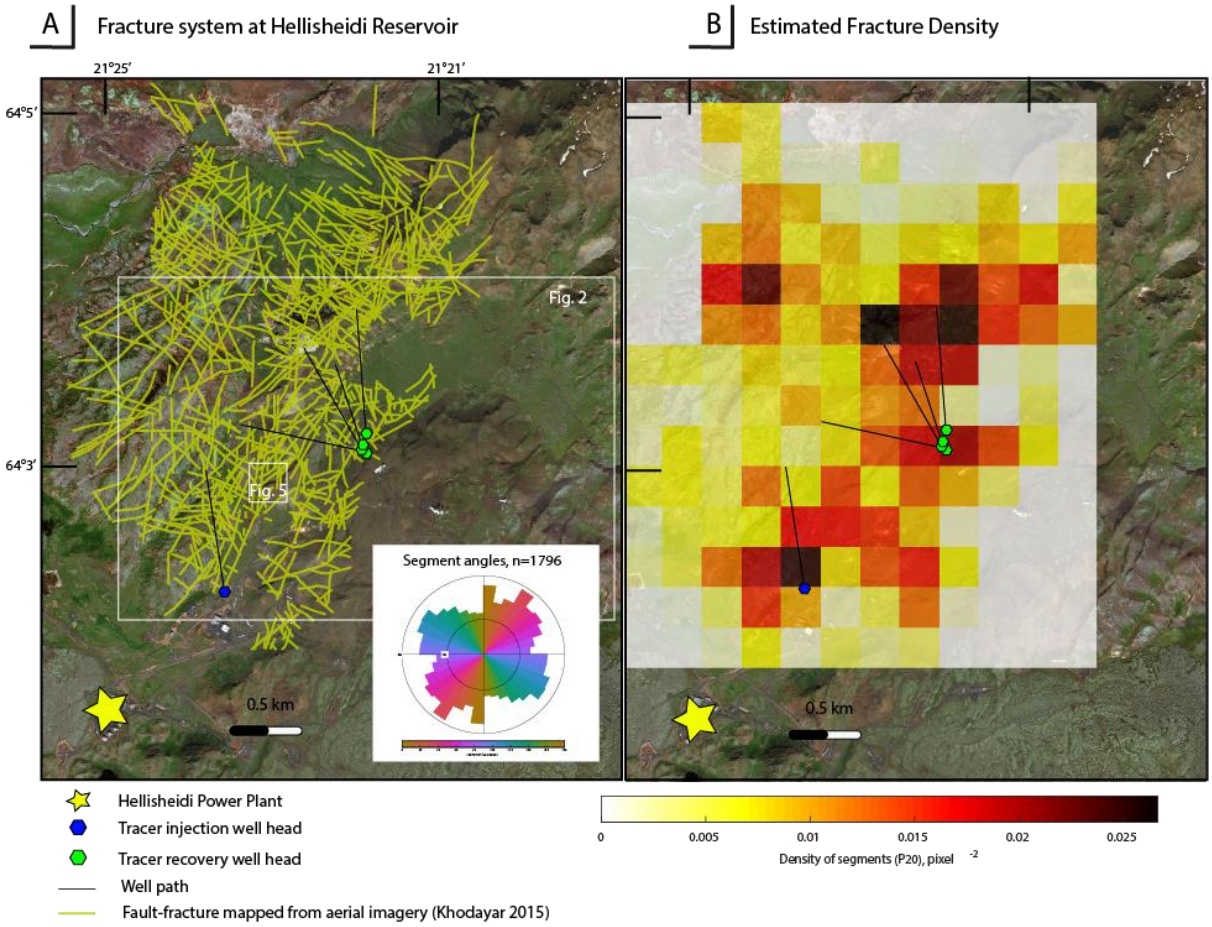

Figure 4: (a) Fracture system at the Husmuli area of Hellisheidi reservoir obtained from aerial imagery by Khodayar (2015) [20]. Fracture strikes, weighted by length, are shown in the rose diagram, indicating the predominance of three major fracture systems: oriented NE-ENE, NS and NW. Tracer injection well and recovery wells are shown in blue and green, respectively. White boxes indicate the location of Figures 2 and 5. (b) Fracture density estimates obtained from fracture pattern analysis toolbox, FracPaQ2D [21]. Fluid flow paths inferred from tracer test results, fracture system orientation, and higher fracture density indicate an ENE-NE trajectory for fluids within the reservoir.

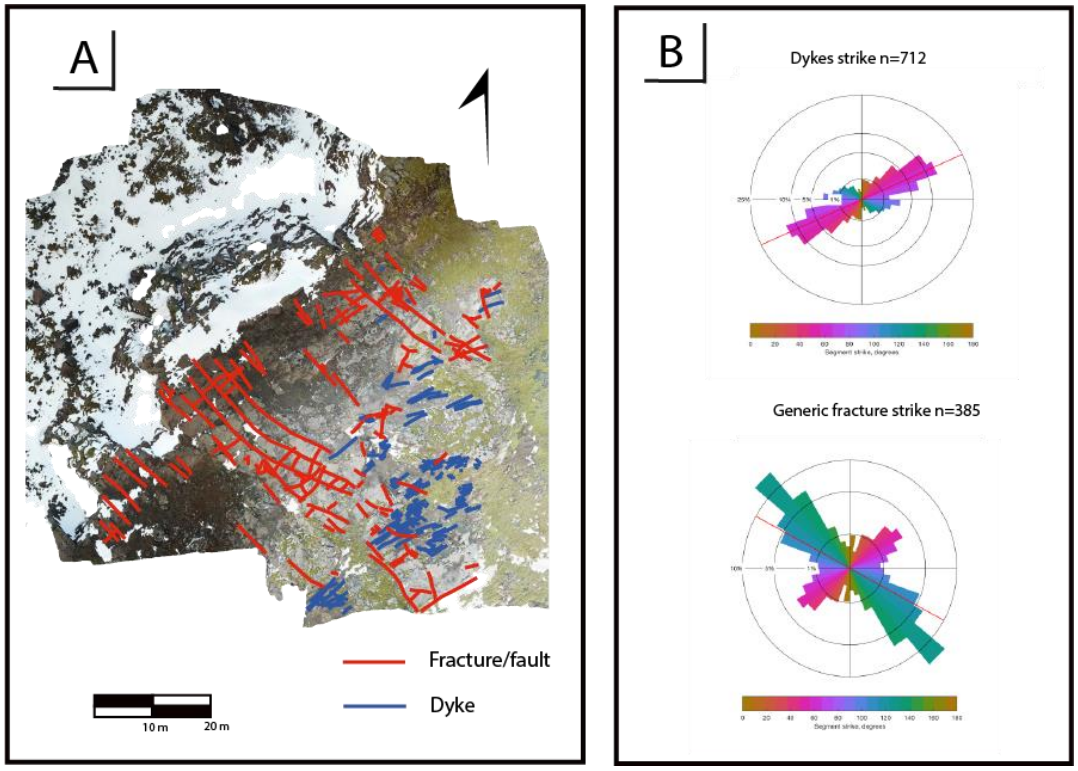

Figure 5: (A) Photogrammetric model obtained from drone imagery of outcrop at location shown in inset in Figure 4. Traced structures (faults, fractures and dykes) were traced manually using Adobe Illustrator. (B) Length-weighted fracture and dykes strike distribution obtained from fracture pattern analysis toolbox [21]. The dominant structure direction is southwest to northeast with a secondary prevalence of NW-SE.

The flow in the studied subsurface basaltic formations resembles a dual porosity fractured model as expressed by the Warren and Root model [24] [8]. Dual porosity flow includes the high accumulation of geothermal fluids in the matrix, favourable rock heat source, and fluid flow through fractures, leads to stable extraction of heat from the reservoir due to high surface area as reported in field observations [25]. For the fracture-matrix transfer function, we used the basic Kazemi et al. (1976) model where the model is considered as a sugar cube with single phase transmissibility [26]. The dual porosity model is consistent with the observation that the injected fluid breaks through rapidly (14 days) but the enthalpy for the produced fluid is steady. The average porosity and permeability of the formation used in the model was obtained from well testing and laboratory experiments [27] and [28], as reported in Table 1. As reported by Houssein (2008) [27], the average permeability-thickness of the Hellisheidi area (estimated from HE-06 well) is about 10.5 Darcy-meter, which was estimated from the well testing information. This parameter can be converted to 87.5 mD of fracture permeability assuming the average thickness of 120 m of gridblocks. Note that, using the reported data in Table 1 as the base input parameters, the distribution of permeability and porosity in the different layers

of the geological model were adjusted using a history matching process to match the tracer tests and information in Table 1.

One important aspect of fractured reservoirs is the notable variations in fracture permeability and porosity due to changes in local effective stress. In the system considered in this study, as injection continues into well HN17 the fracture permeability in vicinity of the injection well is enhanced due to increasing injection pressure, whereas the permeability of producing wells can be reduced due to higher effective stress. To account for this geo-mechanical behaviour, the results of laboratory experiments performed on basaltic rocks were used to model the variation of fracture permeability with respect to effective stress, as illustrated in Figure 6 [28]. In this set of measurements, three parallel fractures were created in a basaltic rock sample [28] [29]. As can be seen in Figure 6, the logarithm of fracture permeability exhibits a linear relationship with effective stress. It should be pointed out that, in the model, the relationship between permeability and effective stress is isotropic and data in Figure 6 was used in the x, y, and z directions. Note that, cold water injection can have significant effects on injectivity and permeability as reported by Gunnarsson G. [30] [31]. However, we did not consider this effect in our modelling due to computational costs caused by this effect.

Table 1: Initial input parameters used to construct the geological model for reservoir simulations.

Average fracture porosity (fraction)	0.01
Average horizontal fracture permeability (m^2)	87.5×10^{-15}
Average vertical fracture permeability (m^2)	87.5×10^{-15}
Fracture spacing (distance between fractures in metres)	50
Matrix porosity (fraction)	0.12
Matrix permeability (m^2)	0.001×10^{-15}

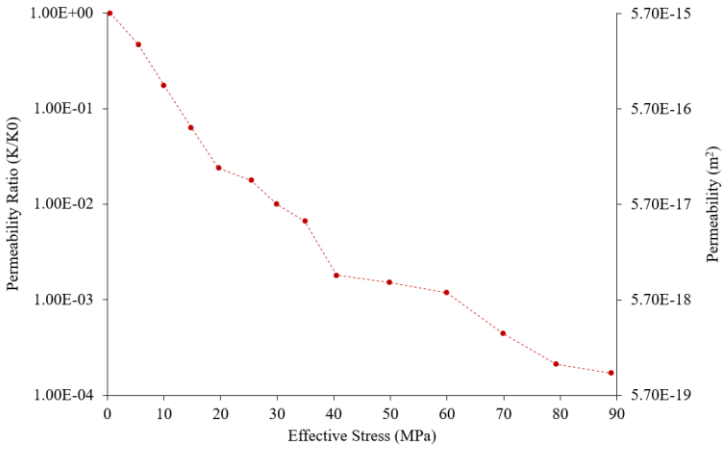

Figure 6: Laboratory measured stress-dependent fractrure permeability of three parallel fractures in basaltic glass samples from the laboratory experiments performed by Nara et al. [28]. Permeability (y-axis) is plotted on a

logrithm scale. The data is converted to a relative permebaility ratio to make the result independent of the intial permeability.

Modelling approach

A dual porosity representation was used to model the reservoir [24]. The 3D distribution and relative magnitudes of horizontal and vertical fracture permeability and fracture porosity within the reservoir were tuned to match the tracer test profiles. Figure 7a illustrates the predominant faults in the Hellisheidi reservoir (highlighted with yellow lines in Figure 7a), which are interpreted to be the primary fluid conduits, as revealed from the tracer test and structural surface mapping. The blue grid blocks in Figure 7a show the constructed fluid flow paths controlling the horizontal and vertical pathways within the reservoir. The other grid blocks in the sector do not contribute to fluid flow. Figure 7b shows the contour line expression of the fracture permeability distribution, with the three faults acting as flow paths due to their higher porosity and permeability compared to the surrounding medium. The base permeability of the fracture network is 87.5 mD [27] and the map on Figure 7b shows the contour map of permeability calculated by averaging the neighbouring grid-blocks. The initial permeability distribution is similar to that of the fracture network shown in Figure 7a, with constant fracture permeability of 87.5 mD for the blue region of Figure 7a, the rest of the model has fracture permeability of 0.5 mD. For the distributed permeability, the two faults on the left were combined and extended to be consistent with the identified fluid flow toward the north of the reservoir. This conceptual gridding scheme was also applied on the southern part of the study area to allow the sector to communicate with southern and northern part of the system, if necessary. Note that the permeability distribution is the initial guess for the model; permeability and porosity of the fracture network is subsequently adjusted by history matching process.

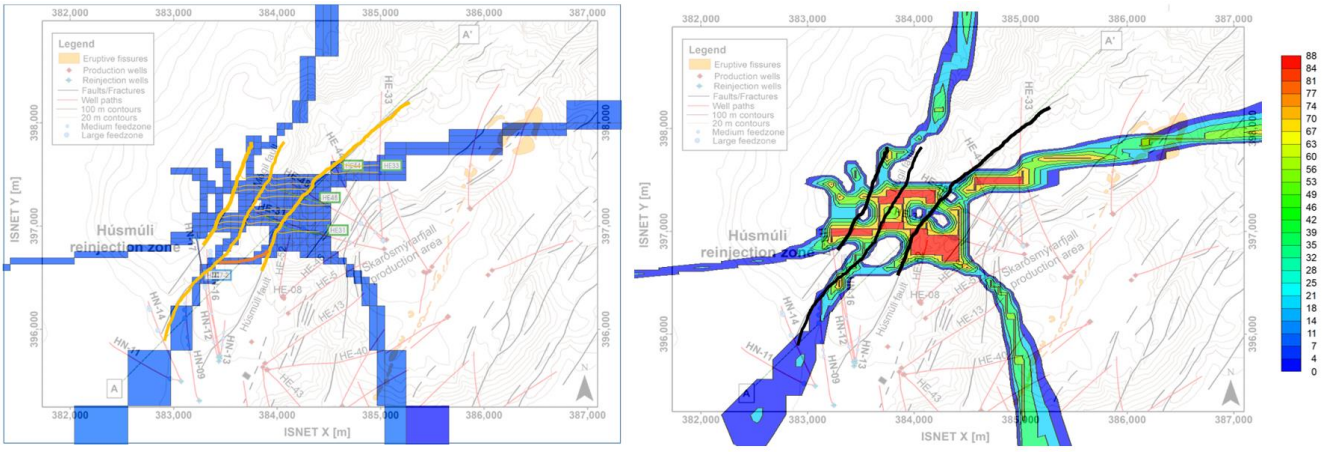

(a) (b)

Figure 7: (a) Schematic illustration of the fluid flow paths based on the inferred fracture network as shown in Figure 5. (b) Fracture permeability distribution in the model represents the three main flow paths (the colour bar shows the fracture permeability). Yellow lines on (a) highlight the three main flow path inferred from fault and dikes exposed in the surface mapping. Black lines on (b) represent the three main fracture permeability flow paths constructed in the geological model. The colorbar in (b) quantifies fracture permeability distribution.

In terms of vertical geological structure, the model has main 7 horizontal layers based on the feedzone depths identified during well testing and target layers for injection and production. The thickness of the layers is based on the depth of the large feedzones, as shown in Figure 3b. This 7-layer model is consistent with the vertical geological structure of the hydrothermal system, where lithological variations between horizontal lava flows and hyaloclastite formations are often intercalated [17]. Figure 8 illustrates the vertical gridding of the model as a function of depth.

The geomechanical properties (i.e. elastic modulus, poison ratio) of matrix and fracture were identical, which are obtained from rock properties of Krafla region published by Eggertsson (2019) [32]. To initialise the geomechanical properties of the model, the effective stress within the reservoir was uniformly distributed. The model has the capability to initialise the pressure and stress fields separately. Hence, the effective stress of the reservoir was set constant as zero to represent a stress dependent permeability ratio of 1 for the entire reservoir (see Figure 6). Although, real reservoirs can exhibit various effective stress distributions, our model is aimed to capture the changes in the stress field due to injection and the initial stress field can not affect the results significantly. That is, the evolution of stress distribution due to injection is the primary controller for the resultant permeability ratio. The initial fluid pressure was distributed vertically based on the gravitational equilibrium using the base water density of 750 kg/m3. The fluid pressure of the top layer was set at 12 MPa based on well testing data [33]. As the pressure distribution was vertically equilibrated, the effective stress distribution would not be altered due to gravitational equilibration. To ensure stable pressure and stress field distribution, the model was run under zero injection and production, which confirmed the equilibrium initial conditions.

Fracture permeability and porosity in the seven horizontal layers were adjusted to history match the field tracer test results. A set of multipliers defined for horizontal (longitudinal) and vertical (transverse) permeabilities were tuned to these results. The multiplier for horizontal and vertical permeability could vary between 0 and 20 (maximum resultant permeability can be 1500×10^{-15} m^2). Additional multipliers were used to account for the fracture permeability of the three main flow paths as highlighted in Figure 7b. The flow paths and corresponding multipliers were tuned for flow between HN17 and HE31, but not for the other producing wells.

In total, 27 parameters (7 longitudinal permeability, 7 transverse permeability, 7 porosity multipliers, 6 additional multipliers for permeability and porosity of three paths) were used for the history matching process.

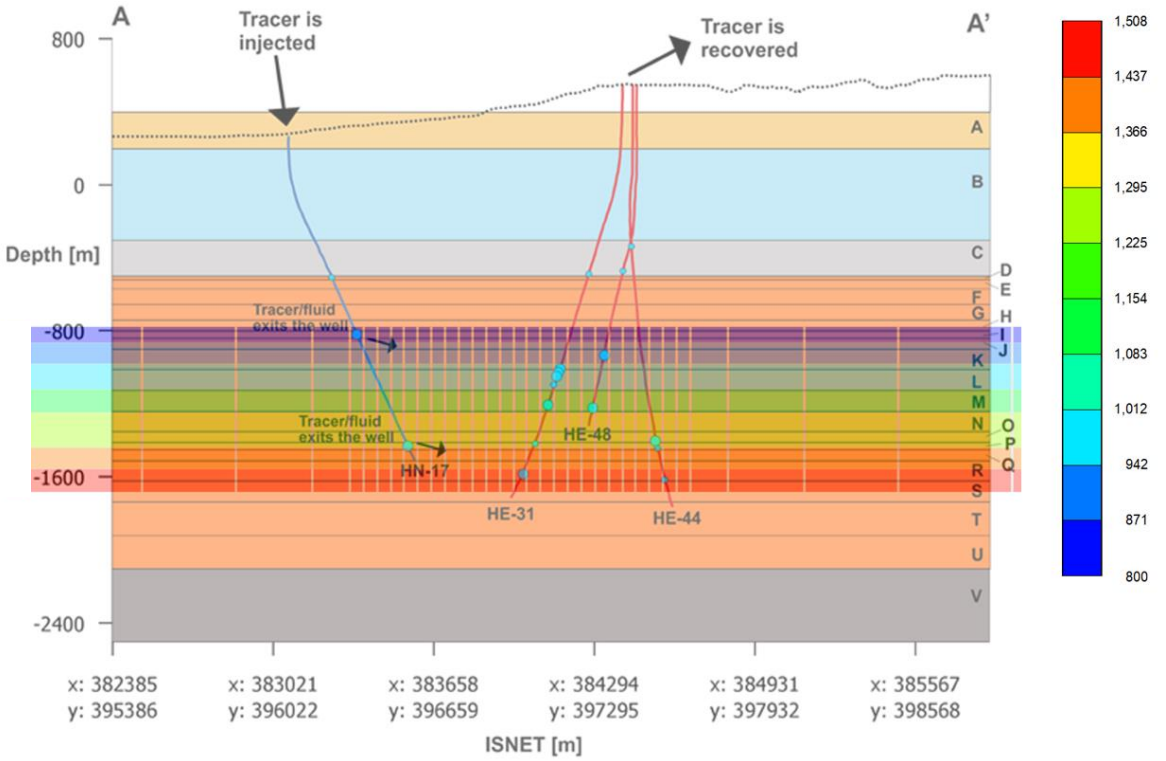

Figure 8: The reservoir sector was divided in 7 layers based on the observed large feedzones, which is superimposed on Figure 3b. The colour bar shows the depth of the layers from 800 down to 1600 metres.

The objective function for the optimisation exercise was the summation of errors in the tracer concentration between simulation and field data. Using CMG Designed Exploration and Controlled Evolution (CMG's proprietary algorithm, which is an improved genetic algorithm) for minimization of objective functions, the reservoir simulator was coupled with the optimizer to estimate the permeability and porosity distribution. This optimization algorithm is based on estimation of the posterior probability function of a parameter [34] [35] [36] [37] [38]. It should be pointed out that CMG-GEM (fully coupled hydro-thermo-mechanical-chemical model) was used as the reservoir simulator. The geo-mechanical package of this software was used for history matching the tracer test results. The modelled fluid is a single-phase liquid water and includes provision for stress-dependent fracture permeability. For history matching, the geochemistry package was not used since the effects of geochemical interactions on flow paths are likely to be insignificant during the 200-day period of the tracer test. However, once the observations of tracer test were matched, the geochemistry package was used for the long-term study of the reservoir performance.

History matching results

Figure 9 depicts the results of history matching for the four producing wells. A good similarity between the simulation results and field data, with a root-mean-square error of 0.94%, was achieved. Not only did the temporal profiles of tracer concentration match well, the arrival time of the tracer in each producing was accurately reproduced. The success of the history matching suggests that the model is suitable for longer-term predictions. The temperature profile for the producers is a flat line showing the reservoir temperature. This agrees with the field data where the produced fluids have a stable temperature on the surface [39] [40] [27]. This set of tracer test was used in other studies for calibrating the flow paths of Husmuli reinjection zone [19] [9] [8]. The previous attempts, however, did not match all the tracer profiles with as high accuracy. Our results demonstrate significant improvement in the quality of the history match. The improvement in our results stems from consideration of geo-mechanics, more tuning parameters, and variable flow properties for geological layers.

To investigate geothermal fluid flow, 3D flow streamlines were generated using the calibrated model as shown in Figure 10. The streamlines are colour coded showing the flow towards the producing wells. From the streamlines (the red streamlines showing flow toward HE31), it can be inferred that the horizontal layers can communicate vertically, i.e. an upward flow of the geothermal fluid is evident. This behaviour of the calibrated model is in agreement with field observations of the vertical communication between in deeper layers [41] [9]. On the other hand, the HE44 well (streamlines in yellow) is fed by downward fluid flow from the top feedzone of HN17 well to the bottom of the feedzone of well HE44 (feedzones refer to perforations at the layers). Therefore, the top and bottom feedzones of HN17 would have a notable vertical flow towards HE44 and HE31, respectively. Figure 11 shows an aerial map of the streamlines towards the producing wells. The calibrated model indicates that the southeast part of the reservoir does not communicate with either well HE31 or the other production wells. This finding is in agreement with the detailed tracer results, where very low quantities of the injected tracer were recovered from the wells located in the south east of the sector [8].

Although the model was designed to capture flow in different directions (see the permeability distribution in Figure 7), the model shows that the predominant flow path is southwest to northeast. Note the HE48 producing well has a similar streamline pattern as well HE31. This similarity between the performance of these wells has been reported elsewhere [20] [9].

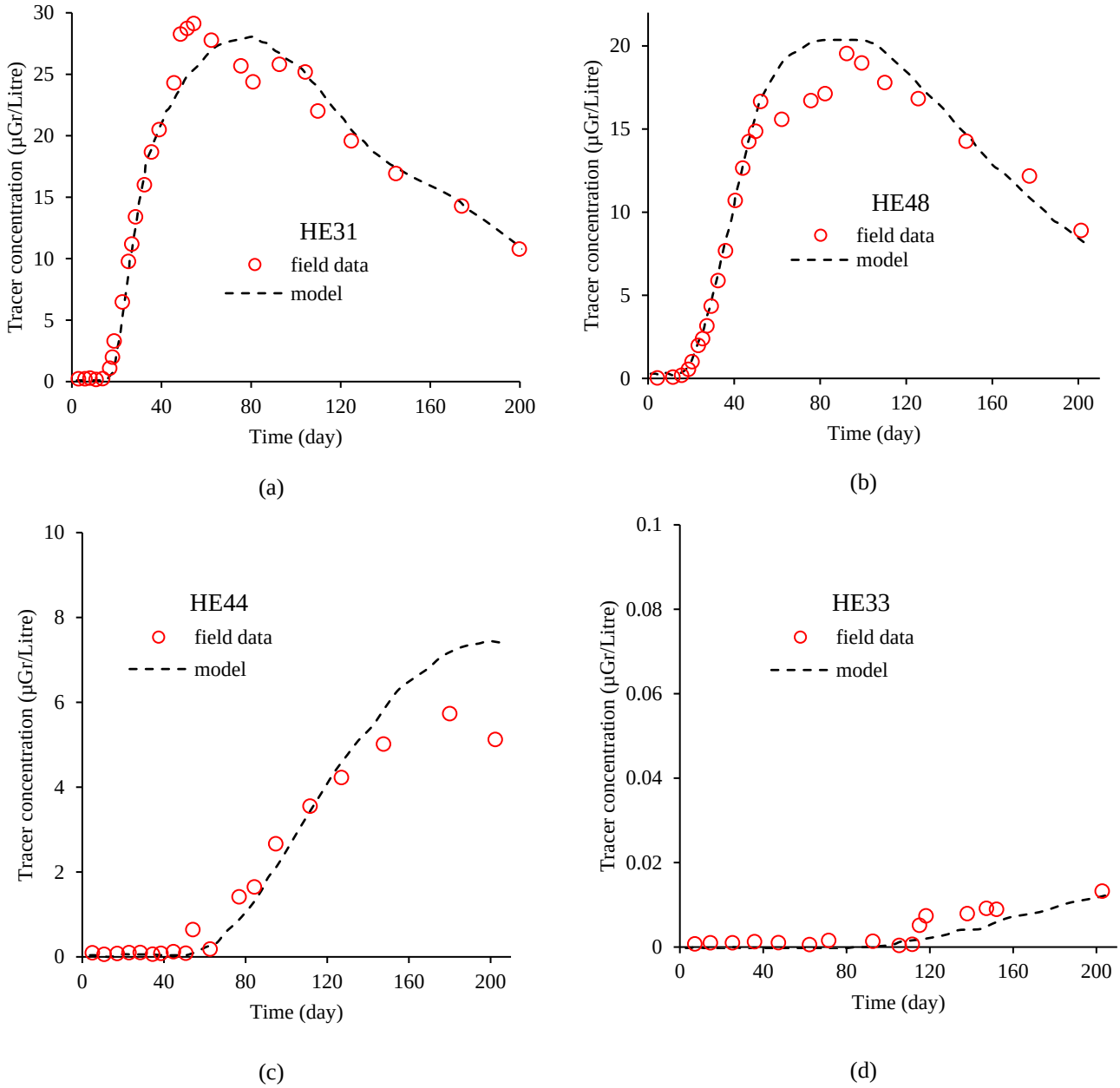

Figure 9: Results of history matching for the four producing wells showing tracer concentrations from field data (open circles) and simulation results (dashed line) for 200 days of the tracer injection. The history matching could attain satisfactory match between filed data and model results for four wells altogether. (a) HE31 well is the nearest well to the injection point with the highest recovery of the tracer. (b) HE48 well has shown the second highest recovery of the tracer, which can be attributed to the extent of this well intercepting the northern two faults. As these two wells behave similarly in terms of arrival time of tracer and amount of tracer recovery, it is likely that, these two wells have separate paths from the injector. (c) HE44 located beyond the HE48 with noticeable drop in the tracer recovery, i.e. maximum of 6 micro-gram/litre compared to 20 micro-gram/litre in HE48. (d) HE33 is the farthest well with lowest amount of tracer recovery.

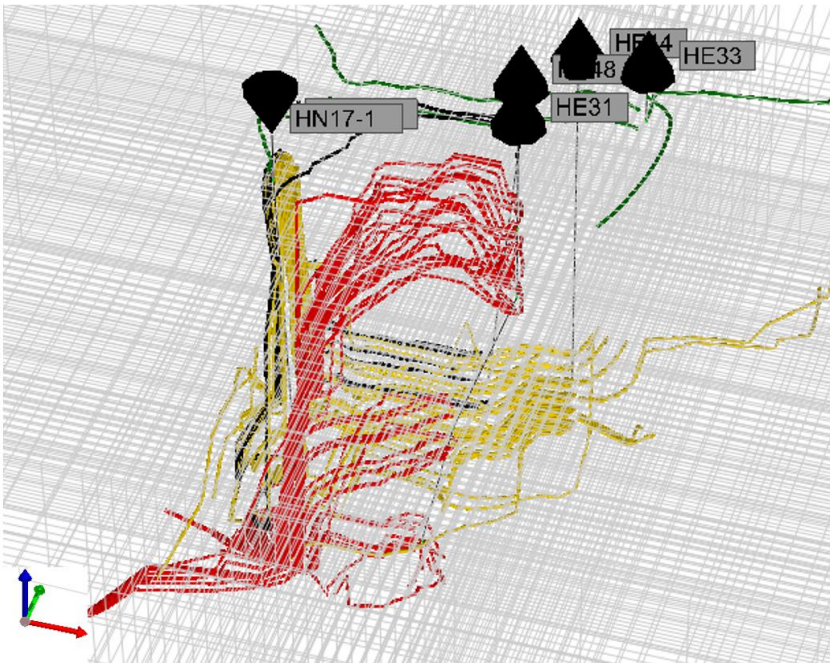

Figure 10: 3D streamlines of the fluid flow paths towards four producing wells. Red, yellow, black, and green streamlines represent flow towards wells HE31, HE48, HE44, and HE33, respectively. Red streamlines of flow towards HE31 indicating an upward flow of the geothermal to top feedzones. It can be seen that two main streamlines take place; one is direct horizontal red streamlines and one upward bunch of streamlines. Yellow Streamlines of flow towards HE48 indicating less upward flow contribution compared to HE31 and also, flow from top injection feedzone to HE48, i.e., downward yellow streamlines. Black streamlines of flow towards HE44 indicating insignificant downward flux from top layers and hence, the streamlines are mostly horizontal for HE44. Green streamlines of flow towards HE33 has no upward flow indicated, and the flux limited to top layer. The scale of the images is similar to that of Figure 11. The black cones on the top of the image represents the wellheads; cones with upward and downward tips represent producing and injecting wells, respectively.

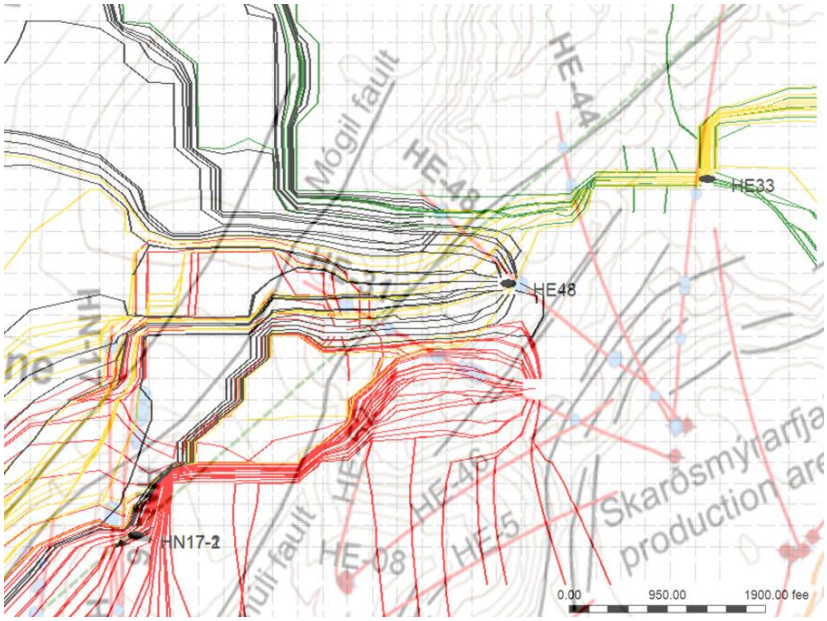

Figure 11: 2D streamlines of the flow towards the four producing wells in layer 1 (the top layer). Red, black, yellow, and green streamlines represent flow towards wells HE31, HE48, HE44, and HE33, respectively. The streamline map is superimposed on the geological map of the region.

Vertical distributions of fracture properties

Figure 12a shows the multipliers for longitudinal (horizontal) fracture permeability for the various layers obtained by matching the model to the tracer test results. These multipliers determine the relative speed of the tracer travelling towards the producing wells in each layer. Fracture permeabilities for different layers vary notably. The fracture permeabilities for layers 5 and 7 are noticeably higher than the others. Also, layer 6 has a relatively high horizontal permeability. This layer is one of the main feedzones by the injection wells as reported by [8]. Figure 12b illustrates the multipliers for vertical fracture permeabilities tuned for the layers. This parameter indicates the vertical communication between the layers. The layers next to the main injection feedzones have high vertical fracture permeabilities that allow the injected tracer to flow across the layers [42].

Figure 12c illustrates the fracture porosity tuned for each reservoir layer. Based on history matching, the reservoir has two distinct compartments. The top of the reservoir has a higher fracture porosity compared to the bottom. This feature provides insight for the further development of the reservoir. This higher fracture porosity could provoke greater mixing between injection and formation fluids, which can lead to higher resident times for the injection fluid to interact with the formation rock and fluids. For example, injection of water into layer 5 layer would benefit from high longitudinal permeability easing the flow and also, high transverse permeability and fracture porosity of the above layer would bring about favourable mixing.

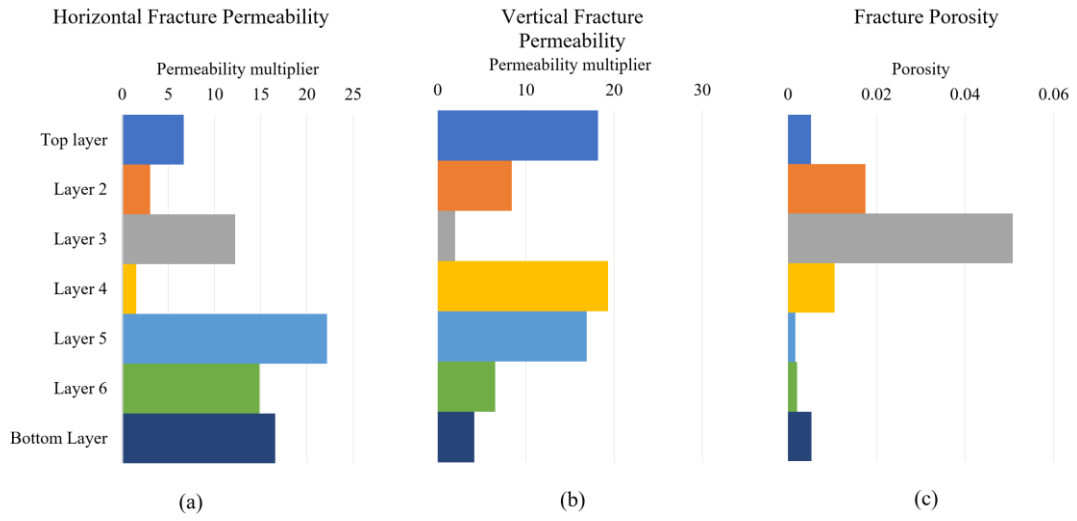

Figure 12: (a) The multipliers for horizontal (longitudinal) fracture permeability obtained from history matching. (b) The multiplier for vertical (transverse) fracture permeability obtained from history matching. (c) Tuned fracture porosities obtained from history matching.

Spatial distribution of fracture properties

Three main fluid flow paths were identified based on geological observations and the temporal tracer recovery profiles. The relative contributions of the fluid flow paths needed adjustment to match the tracer profiles. The fracture porosity and permeability of these fluid flow paths were tuned to the properties of the seven layers. For the spatial distribution of the fracture porosity, five different regions were considered: the three main flow paths between the injection well and HE31, the area between wells HE31 and HE48, and the area between wells HE48 and HE44. However, for the spatial fracture permeability distribution, three main flow paths between the injection well and well HE31 were adjusted.

Figure 13 and Figure 14 illustrate the spatial distributions of fracture porosity and fracture permeability, respectively, optimized by history matching of the tracer test results. The outcome of history matching indicates that the southern fracture path has higher porosity and lower permeability whereas, the northern flow path consists of a low porosity and high permeability fracture network. Based on the calibrated model, two northwest trending faults would have high fracture permeability contributing to the fluid flow of geothermal fluid. Therefore, given the results of areal and vertical fracture distribution, injection into the two northwest trending faults intercepting layers 4 and 5 can be considered as the sweet spot for sustainable flow and hence, heat extraction.

The calibrated model has manifested a notable degree of communications between the faults, which is highlighted in Figure 14 by black arrows. This can also be inferred from the geological interpretation of the faults and the well feedzones; the major feedzones of well HE31 and HE48 are located on the south-east fault and hence, it is plausible that the fluid injected at HN17 could flow towards the south-east fault leading to the producing wells. This finding of the modelling results is in agreement with the geological interpretation of the tracer test whereby the tracer can have a fast travel time to arrive at HE31 in 14 days, which can be satisfy with the considerable communications between faults. In other words, the 3D dual porosity model calibrated on the tracer tests could identify the fractures or smaller faults establishing fault communications between major faults as well as the inter-layer flow streamlines.

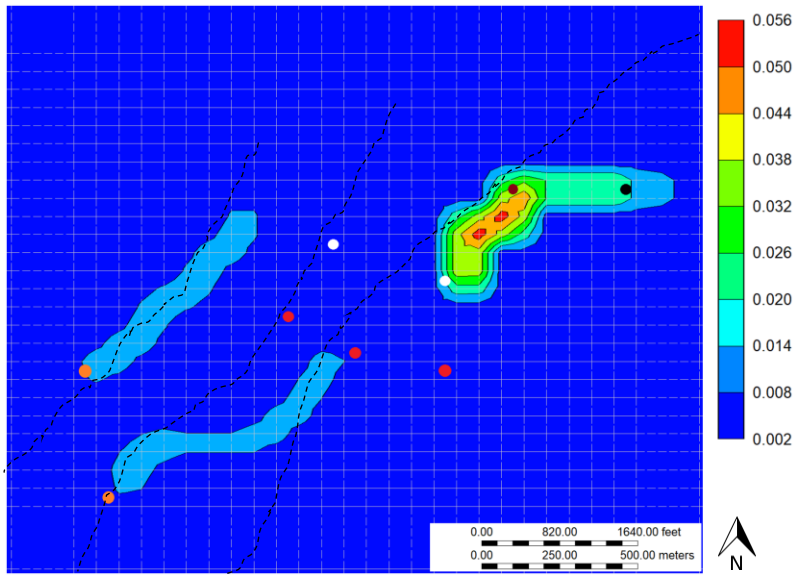

Figure 13: Areal fracture porosity distribution. The green regions represent high fracture porosity whereas, the blue regions indicate low fract ure porosity. The higher the porosity, the higher the mixing between the injected and resident fluids. The production (HE31, HE48 , HE44, and HE33) and reinjection (HN17) well feed-zones are denoted by red, white, brown, black and orange dots, respectively.

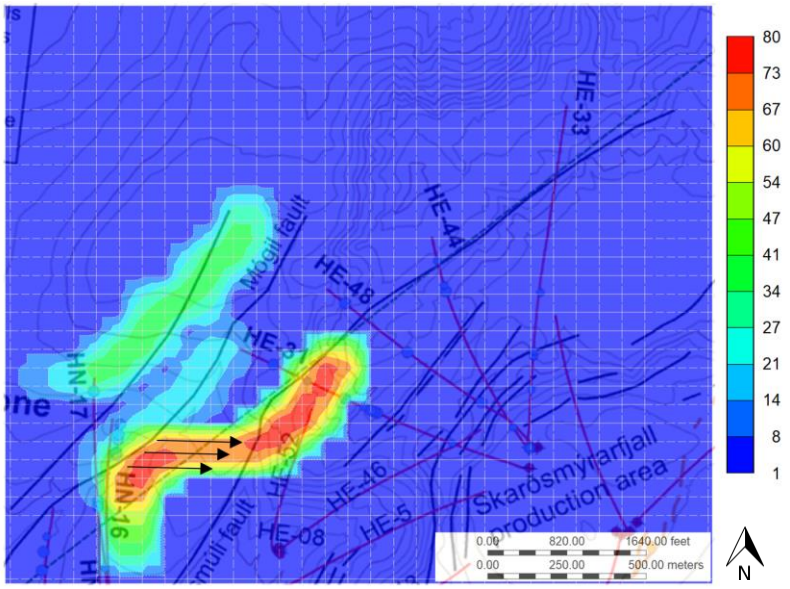

Figure 14: For the three main flow paths, the multipliers for fracture permeability obtained from history matching are illustrated. Two northwest trending faults (with green colour) have higher permeability. The black arrows represent notable communications between two faults. The location of the well perforations and their subsurface traces are shown in red.

Impact of stress dependent permeability

The new model developed for the flow path calibration has benefitted from the laboratory data of stress-dependent permeability. The geomechanics or stress-dependent parameters can be essential for the Hellisheidi reservoir as subsurface models indicate a fracture dominated fluid flow and hence, as shown in Figure 6, the permeability can be impacted 3 orders of magnitude by effective stress. Inclusion of stress field and its consequent equations increased the

simulation run time noticeably. Therefore, for an optimisation run where hundreds of simulations are required, the total time of history matching was increased considerably. To demonstrate the impact of geomechanics on the tracer test modelling, the calibrated model presented in the previous section was re-run with no geomechanics involved to highlight the importance of stress-dependent fracture permeability. To sensitise the model, all the reservoir properties and tuned parameters were kept the same as the calibrated model but the geomechanics was de-coupled.

Figure 15 shows the results of field data for the tracer test performed on HN17 well as compared to the modelling outcome for two models; with no geomechanics and fully coupled hydro-thermo-geomechanics. Decoupling stress-dependent permeability changed the modelling results significantly, which highlights the importance of inclusions of geomechanics in calibrating the fluid flow paths. As highlighted in Figure 15, if the geomechanics are disregarded, the arrivals of the tracer at two adjacent wells in a row (HE31 and HE48) are delayed notably. The delay is higher for the farther well, i.e. HE48. This significant difference in the arrival times can be attributed to the enhanced fractured permeability in the vicinity of the injection well controlled by the stress-dependent parameters. When the local increased stress around the injections well is ignored, the intrinsic fracture permeability could delay the tracer advancement throughout the reservoir. In addition to the arrival time, the concentrations of the tracer recovered at the production wells are considerably lower for the hydro-thermo model.

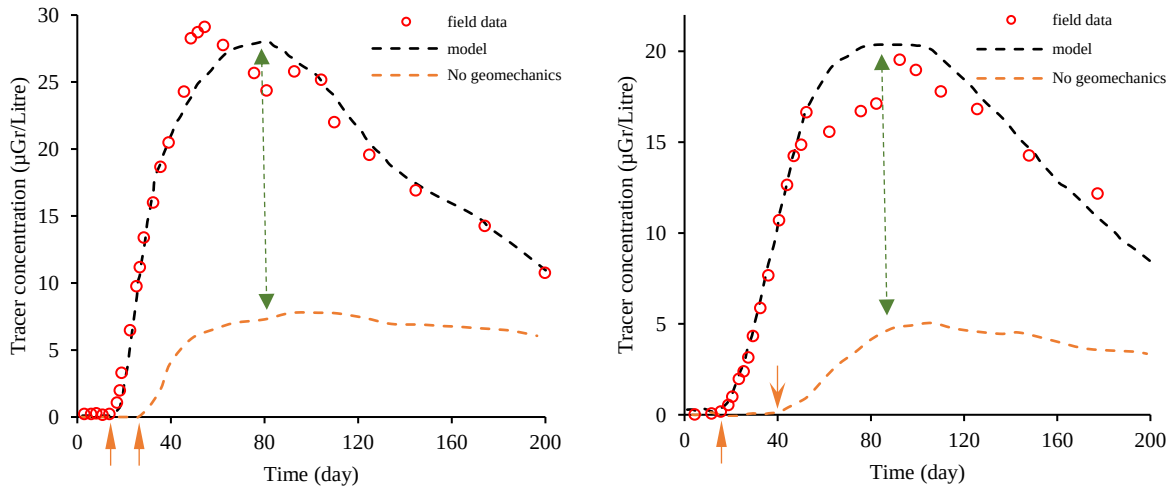

Figure 15: The temporal profiles of the tracer recovery at (a) HE31 well and (b) HE48 well as obtained from field data and modellings. Two cases for modelling were performed; with geomechanics (as indicated by "model") and no geomechanics. When the calibrated model was rerun discarding geomechanics, the arrival time of the tracer was significantly delayed as highlighted by orange arrows as well as the decreased concentrations of the tracer highlighted by the green arrows.

Having shown the impact of geomechanics on fluid path characterisations, it is worthwhile to perform another history matching for the fluid path calibration using a model with no geomechanics involved. Note that the previous part was the calibrated model sensitivity on geomechanics. It is aimed to perform a new calibration without stress-dependent permeability. The same software and optimisation algorithms were incorporated. The reservoir properties were initialised identically, but the stress-dependent parameters were discarded. The history matching was run until the match between the model results and field data was similar to what was achieved in Figure 9.

Figure 16 illustrates the tuned fracture properties for two modelling cases after history matching the tracer test. For horizontal fracture permeability, the case with stress-dependent parameters indicates two-zone flow paths separated by layer 4, i.e. layer 1-3 and layer 5-7 behaving as two separate flow units. However, this characteristic of the layers can not be captured. Also, the deep layer (7^{th} layer) would have a very low flow conductivity compared to the model calibrated using the geomechanics. In terms of vertical permeability, the model with the geomechanical process could promote vertical communication between two flow zones controlled by vertical permeability of layers 4 and 5. However, for the no-geomechanics model, vertical communications are diminished. The fracture porosity for both models could exhibit a similar trend except layers 3 and 1. Therefore, the inclusion of the geomechanics could bring about a different calibrated fluid flow regime for fractured-dominant reservoirs. This also can be attributed to the strong correlation between permeability and effective stress as identified from laboratory experiments (see Figure 6) performed on Icelandic basalts. As laboratory and modelling attempts have demonstrated, the stress-dependent phenomena exist and are important in characterisation of the fluid paths and hence, the fluid flow paths should be calibrated by the inclusion of stress-dependent properties.

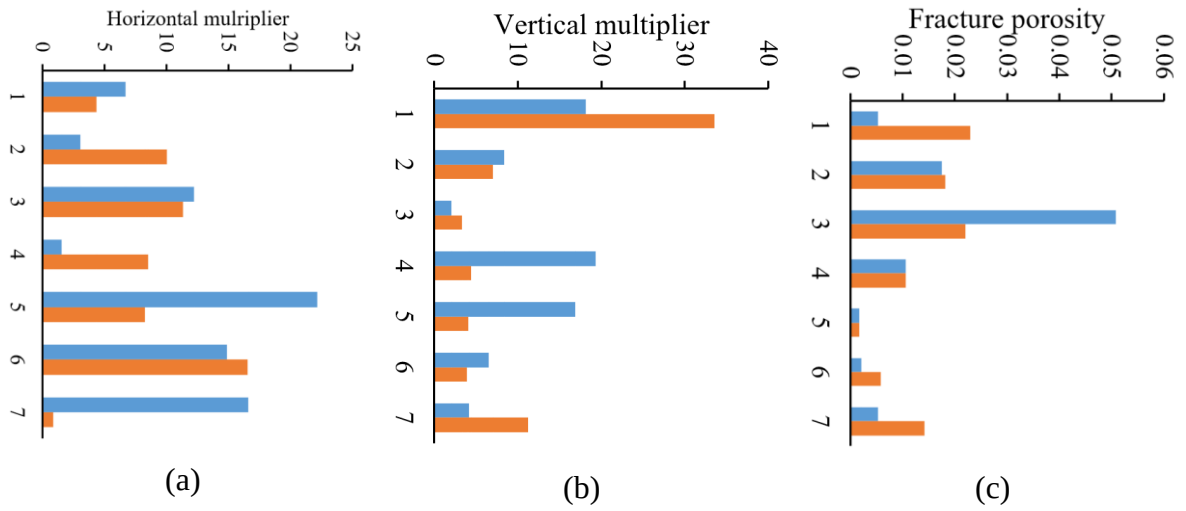

Figure 16: for two history matching cases, with (in orange colour) and without (in blue colour) geomechanics, (a) The multipliers for horizontal (longitudinal) fracture permeability. (b) The multiplier for vertical (transverse) fracture permeability. (c) Tuned fracture porosities. Notable differences can be brought about by the inclusion of the stress-dependent properties.

Validation of fluid path characterisation

The Hellisheidi geothermal plant has been capturing CO_2 and H_2S by their dissolution in pressurized water and re-injecting the gas-charged water into the subsurface basalts for the storage of these gases as part of the CarbFix2 project [43] [44]. The injection of CO_2-charged water into basaltic rocks and the resultant mineralisation of the injected CO_2 to carbonate minerals has been investigated at different scales [43], and the successful mineral storage of CO_2 and H_2S has been demonstrated [14] [45] [46]. In short, CO_2 and H_2S are dominated in aqueous solution as the HCO_3^- and HS^- species, which react with cations such as Ca^{2+} and Mg^{+2} and Fe^{2+} released from basalt dissolution to form of carbonate and sulphites [14]. One crucial challenge for CO_2 storage characterisation as well as geothermal activities is to estimate the predominant flow paths where the mineralisation take place, which can lead to quantify CO_2 mineralisation and the consequent changes in permeability of fracture network over time.

Well HN16 is used for CO_2 fixation project, as highlighted in Figure 17, which is drilled in the same formation as HN17. It is conceivable that the HN17 and HN16 wells share identical flow paths due to similar feedzones for these wells [8]. Therefore, the calibrated fluid flow paths for the tracer test performed on HN17 can be used to model injection into well HN16. As can be seen in Figure 17, the major difference between HN17 and HN16 is the depth of the main feedzones. To validate whether the calibrated model used for the HN17 can be employed to model accurately injections into well HN16, the results of an independent tracer test can be compared against the model results. The aqueous phase re-injected into well HN16 was doped

with a tracer continuously for a period of roughly two years [47]. Note that, the tracer test for HN17 was a batch injection whereas the tracer test for HN16 was a continuous injection. Therefore, these two tracer tests are independent but performed over identical subsurface flow paths. Details of the tracer test performed at HN16 can be found elsewhere [47].

Figure 18 illustrates the results of the observed tracer concentrations in the producing wells compared against the model results of this tracer test. The subsurface model calibrated using HN17 tracer test results was used for the HN16 well properties. Note that the stress-dependent permeability module was incorporated into the model. No tuning was performed and Figure 18 shows the predictive forward model results. The forward model reproduces the field observations with the root-mean-square error below 3.55%. This satisfactory prediction of the independent tracer test validates the tuned model. Note that the quality of the match for continuous tracer test at HN16 is not as good as the batch tracer test at HN17 as can be inferred from the root-mean-square errors, as the latter is a prediction not a fit of the data. Nevertheless, the similarity of field observation and model results is sufficient for validation of the calibrated fluid paths. In other words, our approach of including geomechanics in calibrating the fluid flow path could lead to a reliable model.

In terms of calibration process and selecting the calibrated models, the process of history matching may be affected by non-uniqueness and uncertainty issues. For instance, in the batch tracer test performed on HN17, the tracer profiles for HE31 and HE48 have exhibited double-peaks as can be seen in Figure 3-a, which was not captured by the calibrated model. It should be pointed out that, the double-peak may be affected by measurement uncertainties as well as the geological and natural factors where double-peaks may imply two different paths with different arrival times. The double-peaks and possibility of two paths were mentioned in the reports [19] whereas, other reports may have implied different approach and did not capture the two peak tracer profiles [8]. Therefore, uncertainty and non-uniqueness issues existed in the previous attempts. However, in spite of reaching various calibrated models in our history matching process that could reproduce the double-peaks, our criterion to filter the calibrated models was the ability to reproduce the continuous tracer test at HN16. Therefore, we suggest that one method to alleviate the non-uniqueness issue is to assess the calibrated models against an independent set of field observations such as a tracer test in neighbouring wells.

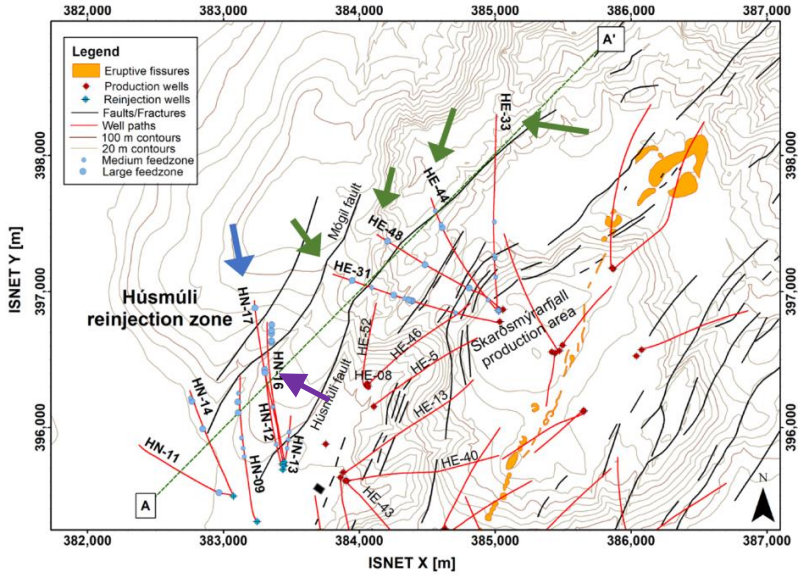

Figure 17: CarbFix2 project has been injecting dissolved CO_2 and H_2S into Hellisheidi reservoir using the HN16 re-injection well as highlighted with a purple arrow. Blue arrow indicates HN17, which was used for batch tracer test and model calibration. Green arrows points to the producing wells used to monitor tracer recovery profiles. The feedzones for HN16 and HN-17 are close to each other, which makes the calibrated model for HN17 useful for modelling of the CO_2 storage project ongoing at HN16.

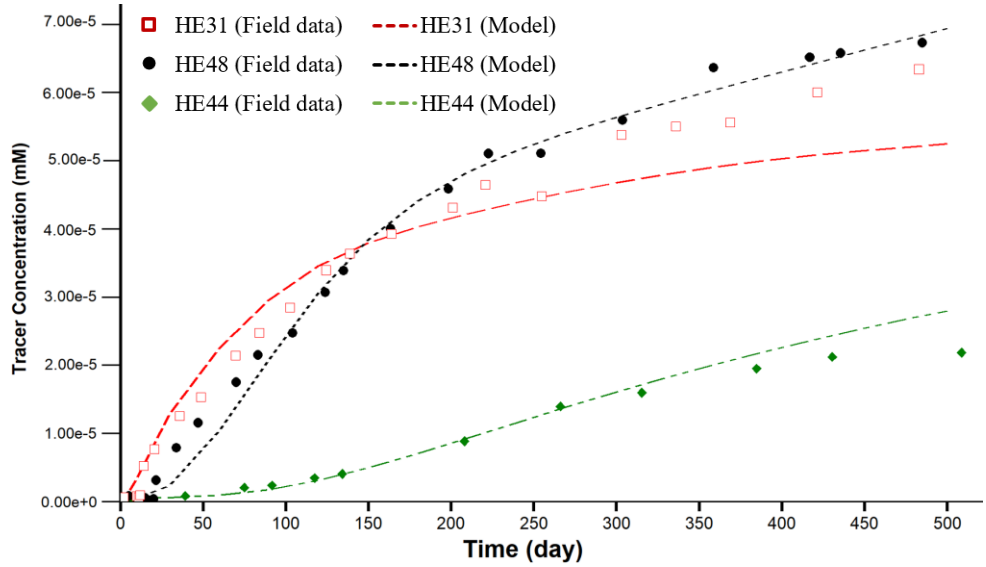

Figure 18: Temporal profiles of the tracer recovery at HE31, HE48, and HE44. The tracer was contineously injected into HN16 for approximately two years and the monitoring samples were collected from the wells to the norteast of the injection well. The field data was obtained from Gunnarson et al. [47].

Conclusions

A series of reservoir model calculations were performed to study coupled hydro-thermo-mechanical-chemical processes in the basaltic Hellisheidi reservoir in Southwest Iceland. The geological model was calibrated to match chemical tracer test results using hydro-thermo-mechanical physics, where stress-dependent fracture permeability was taken into account. The

results revealed the considerable impact of stress-dependent properties for the calibration of flow paths in fractured reservoirs. The fluid flow path in Husmuli area was primarily controlled by the faults. Also, NW-SE intra-communications has been identified between the major faults, which can highlight the propagation of chemicals through the fractures. The modelling results indicated that the geological layers can be compartmentalised into two main fluid paths, which are in agreement with other field observations [41]. Also, the modelling attempts indicated that, the faults are the main conduit for the fluid flow captured by dual porosity model, which could control the fast transport of the tracers. In other words, the injected fluid would mostly travel through the major fractures or the faults, which can have significant implications in terms of the reactive surface area for the ongoing CO_2 fixation project in Husmuli area. Having sensitised the impact stress-dependent properties, it was shown that the inclusion of the geomechanical calculations in history matching of the tracer test can lead to significant improvements in fluid flow path characterisation. The calibrated model could estimate the results of an independent tracer test with acceptable accuracy validating the predictive capability of the model. Overall, the reservoir parameters such as permeability and porosity should be treated as stress-dependent for fracture reservoir for characterisation of the flow paths, which is crucial for identifying the permeable compartments within the reservoir and the development scenarios.

Acknowledgement

This work is part of the Science for Clean Energy research consortium funded by European Union's Horizon 2020 research and innovation programme. For simulations, CMG software from Computer Modeling Group was used, which is appreciated. Also, we like to thank the technical staffs in CMG Europe office for supports in running the simulations.

References

[1] A. Anderson and B. Rezaie, "Geothermal technology: Trends and potential role in a sustainable future," *Applied Energy,* vol. 248, pp. 18-34, 2019.

[2] W. Ruhaak, C. D. Heldmann, L. Pei and I. Sass, "Thermo-hydro-mechanical-chemical coupled modeling of geothermally used fractured limestone," *International Journal of Rock Mechanics and Mining Sciences,* vol. 100, pp. 40-47, 2017.

[3] T. Diehl, T. Kraft, E. Kissling and S. Wiemer, "The induced earthquake sequence related to the St. Gallen deep geothermal project (Switzerland): Fault reactivation and fluid interactions imaged by microseismicity," *J. Geophys. Res. Solid Earth,* vol. 122, pp. 7272-7290, 2017.

[4] S. N. Pandey, V. Vishal and A. Chaudhuri, “Geothermal reservoir modeling in a coupled thermo-hydro-mechanical-chemical approach: A review,” *Earth-Science Reviews,* vol. 185, pp. 1157-1169, 2018.

[5] Z. Qu, W. Zhang and T. Guo, “Influence of different fracture morphology on heat mining performance of enhanced geothermal systems based on COMSOL,” *International Journal of Hydrogen Energy,* vol. 42, pp. 18263-18278, 2017.

[6] T. Doe, R. McLaren and W. Dershowitz, “Discrete Fracture Network Simulations of Enhanced Geothermal Systems,” California, USA, 2014.

[7] J. Rutqvist, “Fractured rock stress-permeability relationships from in situ data and effects of temperature and chemical-mechanical couplings,” *Geofluids,* vol. 15, pp. 48-66, 2015.

[8] T. M. Ratouis, S. Snabjornsdottir, G. Gunnarsson, I. Gunnarsson, B. Kristjansson and E. Aradottir, “Modelling the Complex Structural Features Controlling Fluid Flow at the CarbFix2 Reinjection Site, Hellisheiði Geothermal Power Plant, SW-Iceland,” in *44th Workshop on Geothermal Reservoir Engineering*, California, USA, 2019.

[9] S. Snabjornsdottir, S. Tomasdottir, B. Sigfusson, E. Aradottir, G. Gunnarsson, A. Niemi, F. Basirat, B. Dessirier, S. Gislason, E. H. Oelkers and H. Franzson, “The geology and hydrology of the CarbFix2 site, SW-Iceland,” *Energy Procedia,* vol. 146, pp. 146-157, 2018.

[10] S. Salimzadeh, A. Paluszny, H. M. Nick and R. W. Zimmerman, “A three-dimensional coupled thermo-hydro-mechanical model for deformable fractured geothermal systems,” *Geothermics,* vol. 71, pp. 212-224, 2018.

[11] J. H. Norbeck, M. W. McClure and R. N. Horne, “Field observations at the Fenton Hill enhanced geothermal system test site support mixed-mechanism stimulation,” *Geothermics,* vol. 74, pp. 135-149, 2018.

[12] I. Gunnarsson, E. Aradóttir, B. Sigfússon, E. Gunnlaugsson and B. Júlíusson, “Geothermal Gas Emission From Hellisheiði and Nesjavellir Power Plants, Iceland,” *GRC Transactions,* vol. 37, pp. 785-789, 2013.

[13] S. O. Snabjornsdottir, S. Gislason, I. M. Galeczka and E. H. Oelkers, “Reaction path modelling of in-situ mineralisation of CO2 at the CarbFix site at Hellisheidi, SW-Iceland,” *Geochimica et Cosmochimica Acta,* vol. 220, pp. 348-366, 2018.

[14] J. M. Matter, M. Stute, S. O. Snabjornsdottir, E. H. Oelkers, S. R. Gislason, E. S. Aradottir, B. Sigfusson, I. Gunnarsson, H. Sigurdardottir, E. Gunnlaugsson, G. Axelsson, H. A. Alfredsson, D. Wolff-Boenisch, K. Mesfin, D. F. Taya, J. Hall, K. Dideriksen and W. S. Broecker, “Rapid carbon mineralization for permanent disposal of anthropogenic carbon dioxide emissions,” *Science,* vol. 352, no. 6291, pp. 1312-1314, 2016.

[15] P. Einarsson, “Plate boundaries, rifts and transforms in Iceland,” *Jokull,* vol. 58, pp. 35-58, 2008.

[16] B. S. Hardarson, G. M. Einarsson, B. R. Kristjansson, G. Gunnarsson, H. M. Helgadottir, H. Franzson, K. Arnason, K. Agustsson and E. Gunnlaugsson, “Geothermal Reinjection at the

Hengill Triple Junction, SW Iceland," in *Proceedings World Geothermal Congress*, Bali, Indonesia, 2010.

[17] H. A. Alfredsson, E. H. Oelkers, B. S. Hardarsson, H. Franzson, E. Gunnlaugsson and S. R. Gislason, "The geology and water chemistry of the Hellisheidi, SW-Iceland carbon storage site," *International Journal of Greenhouse Gas Control,* vol. 12, pp. 399-418, 2013.

[18] B. R. Kristjansson, G. Axelsson, G. Gunnarsson, I. Gunnarsson and F. Oskarsson, "Comprehensive Tracer Testing in the Hellisheiði Geothermal Field in SW-Iceland," in *Proceedings 41st Workshop on Geothermal Reservoir Engineering*, California, USA, 2016.

[19] S. Tomasdottir, "Flow paths in Husmuli reinjection zone, Iceland," Masters Thesis, Department of Earth Sciences, Uppsala University, Uppsala, 2018.

[20] M. Khodayar, G. Axelsson and B. Steingrimsson, "Potential Structural Flow Paths for Tracers and Source Faults of Earthquakes at Húsmúli, Hengill, South Iceland," report ÍSOR-2015/035, Reykjavík: ISOR, 2015.

[21] D. Healy, R. E. Rizzo, D. G. Cornwwall, N. J. Farrell, H. Watkins, N. E. Timms, E. Gomez-Rivas and M. Smith, "FracPaQ: A MATLAB™ toolbox for the quantification of fracture patterns," *Journal of Structural Geology,* vol. 95, pp. 1-16, 2017.

[22] M. Mauldon, W. M. Dunne and M. Rohrbaugh, "Circular scanlines and circular windows: new tools for characterizing the geometry of fracture traces," *J. Struct. Geol.,* vol. 23, no. 2, pp. 247-258, 2001.

[23] S. F. Cox and K. Ruming, "The St Ives mesothermal gold system, Western Australia—a case of golden aftershocks?," *Journal of Structural Geology,* vol. 26, pp. 1109-1125, 2004.

[24] J. E. Warren and P. J. Root, " The Behavior of Naturally Fractured Reservoirs," *SPE Journal,* vol. 3, no. SPE-426-PA, pp. 245-255, 1963.

[25] G. Gunnarsson, A. Arnaldsson and A. L. Oddsdottir, "Model simulations of the geothermal fields in the Hengill area, South-western Iceland," in *World Geothermal Congress*, Bali, Indonesia, 2010.

[26] H. Kazemi, L. S. Merrill and K. L. Porterfield, "Numerical Simulation of Water-Oil Flow in Naturally Fractured Reservoirs," *SPE Journal,* vol. 16, p. 317–326, 1976.

[27] D. E. Houssein, "GEOTHERMAL RESOURCE ASSESSMENT THROUGH WELL TESTING AND PRODUCTION RESPONSE MODELLING," MSc thesis, Department of Mechanical and Industrial Engineering, University of Iceland, Orkustofnun, Grensásvegur 9, IS-108 Reykjavík, Iceland, 2008.

[28] Y. Nara, P. G. Meredith, T. Yoneda and K. Kaneko, "Influence of macro-fractures and micro-fractures on permeability and elastic wave velocities in basalt at elevated pressure," *Tectonophysics,* vol. 503, pp. 52-59, 2011.

[29] H. S. Vik, S. Salimzadeh and H. M. Nick, “Heat recovery from multiple-fracture enhanced geothermal systems: The effect of thermoelastic fracture interactions,” *Renewable Energy,* vol. 121, pp. 606-622, 2018.

[30] G. Gunnarsson, “Temperature Dependent Injectivity and Induced Seismicity—Managing Reinjection in the Hellisheiði Field, SW-Iceland,” *GRC Transactions,* vol. 37, pp. 1019-1026, 2013.

[31] G. Gunnarsson, “MASTERING REINJECTION IN THE HELLISHEIDI FIELD, SW-ICELAND: A STORY OF SUCCESSES AND FAILURES,” in *Thirty-Sixth Workshop on Geothermal Reservoir Engineering*, Stanford University, Stanford, California, 2011.

[32] G. . H. Eggertsson, Constraining mechanical and permeability properties of the Krafla geothermal reservoir, North-East Iceland, University of Liverpool: Thesis for Doctor of Philosophy, 2019.

[33] G. Bjornsson, “RESERVOIR CONDITIONS AT 3-6 KM DEPTH IN THE HELLISHEIDI GEOTHERMAL FIELD, SW-ICELAND, ESTIMATED BY DEEP DRILLING, COLD WATER INJECTION AND SEISMIC MONITORING,” in *PROCEEDINGS, Twenty-Ninth Workshop on Geothermal Reservoir Engineering*, Stanford, California, 2004.

[34] M. Akbarabadi, M. Borges, A. Jan, F. Pereira and M. Piri, “A bayesian framework for the validation of models subsurface flows: synthtic experiments,” *Computational Geoscience,* vol. 19, pp. 1231-1250, 2015.

[35] P. Mahzari, A. AlMesmari and M. Sohrabi, “Co-history Matching: A Way Forward for Estimating Representative Saturation Functions,” *Transport in Porous Media,* vol. 125, no. 3, pp. 483-501, 2018.

[36] P. Mahzari, A. P. Jones and E. H. Oelkers, “An integrated evaluation of enhanced oil recovery and geochemical processes for carbonated water injection in carbonate rocks,” *Journal of Petroleum Science and Engineering,* vol. 181, p. 106188, 2019.

[37] P. Mahzari and M. Sohrabi, “A Robust Methodology To Simulate Water-Alternating-Gas Experiments at Different Scenarios Under Near-Miscible Conditions,” *SPE Journal,* vol. 22, pp. 1506 - 1518, 2017.

[38] P. Mahzari and M. Sohrabi, “An improved approach for estimation of flow and hysteresis parameters applicable to WAG experiments,” *Fuel,* vol. 197, pp. 359-372, 2017.

[39] M. R. Abad, “RESERVOIR PARAMETERS FOR WELL HE-5, HELLISHEIDI GEOTHERMAL FIELD, SW-ICELAND,” number 18 of the UNU-GTP (Reports 2003), Orkustufnun, 2003.

[40] D. Elmi and G. Axelsson, “APPLICATION OF A TRANSIENT WELLBORE SIMULATOR TO WELLS HE-06 AND HE-20 IN THE HELLISHEIDI GEOTHERMAL SYSTEM, SW-ICELAND,” in *Thirty-Fourth Workshop on Geothermal Reservoir Engineering*, Stanford University, Stanford, California, 2009.

[41] H. Franzson, E. Gunnlaugsson, K. Árnason, K. Sæmundsson, B. Steingrímsson and B. Harðarson, "The Hengill Geothermal System, Conceptual Model and Thermal Evolution," in *Proceedings World Geothermal Congress*, Bali, Indonesia, 2010.

[42] B. M. Thien, G. Kosakowski and D. Kulik, "Differential alteration of basaltic lava flows and hyaloclastites in Icelandic hydrothermal systems," *Geothermal Energy,* vol. 3, no. 11, pp. 1-32, 2015.

[43] S. Gislason, H. Sigurdardottir, E. Aradottir and E. H. Oelkers, "A brief history of CarbFix: Challenges and victories of the project's pilot phase," *Energy Procedia,* vol. 146, pp. 103-114, 2018.

[44] S. O. Snæbjörnsdóttir, B. Sigfússon, C. Marieni, D. Goldberg, S. R. Gislason and E. H. Oelkers, "Carbon dioxide storage through mineral carbonation," *Nature Reviews Earth & Environment,* vol. 1, pp. 90-102, 2020.

[45] R. Trias, B. Menez, P. Campion, Y. Zivanovic, L. Lecourt, A. Lecoeuvre, P. Schmitt-Kopplin, J. Uhl, S. Gislason, H. Alfredsson, K. Mesfin, S. Snabjornsdottir, E. Aradottir, I. Gunnarsson, J. Matter, M. Stute, E. H. Oelkers and E. Gerard, "High reactivity of deep biota under anthropogenic CO2 injection into basalt," *Nature Communications,* vol. 8, p. 1063, 2017.

[46] E. H. Oelkers, R. Butcher and P. Pogge von Strandmann, " Using stable Mg isotope signatures to assess the fate of magnesium during the in situ mineralisation of CO2 and H2S at the CarbFix site in SW-Iceland," *Geochemica et Cosmochimica Acta,* vol. 245, pp. 542-555, 2018.

[47] I. Gunnarsson, E. Aradottir, E. H. Oelkers, D. Clark, M. Arnarson, B. Sigfusson, S. Snabjornsdottir, J. Matter, M. Stute, B. Juliusson and S. Gislason, "The rapid and cost-effective capture and subsurface mineral storage of carbon and sulfur at the CarbFix2 site," *International Journal of Greenhouse Gas Control,* vol. 79, pp. 117-126, 2018.

[48] O. K. Zakharova and V. V. Spichak , "Geothermal fields of Hengill Volcano, Iceland," *Journal of Volcanology and Seismology,* vol. 6, p. 1–14, 2012.